frontiers | Frontiers in Catalysis

ORIGINAL RESEARCH
published: 08 June 2022
doi: 10.3389/fctls.2022.914670

Biodiesel Production From Oleic Acid Using Biomass-Derived Sulfonated Orange Peel Catalyst

*Manoj Kumar Kumawat and Samuel Lalthazuala Rokhum**

Department of Chemistry, National Institute of Technology, Silchar, India

Biodiesel, as an alternative fuel for petroleum-based fuel, has recently acquired significant attention. The current study focused on using biowaste to produce catalysts for low-cost biodiesel manufacturing. Orange peels (OP) were used to make carbon-based solid acid catalysts with sulfonic acid group (–SO_3H) density of 1.96 mmol g^{-1} *via* a "one-pot" carbonization-sulfonation treatment. Under the optimized reaction conditions (15:1 MeOH to oleic acid molar ratio, 7 wt.% catalyst loading w.r.t oleic acid, 80°C reaction temperature, 60 min reaction time), 96.51 ± 0.4% conversion of oleic acid to methyl oleate (a biodiesel component) was obtained. The catalyst displayed high recyclability and stability on repeated reuse, with a negligible decrease in biodiesel conversion up to 5 catalytic cycles.

Keywords: biodiesel, renewable energy, esterificaiton, biogenic, sulfonation

OPEN ACCESS

Edited by:
Putla Sudarsanam, National Chemical Laboratory (CSIR), India

Reviewed by:
Hu Li, Guizhou University, China
Jimmy Nelson Appaturi, Universiti Sains Malaysia (USM), Malaysia
Saikat Dutta, National Institute of Technology, Karnataka, India

****Correspondence:***
Samuel Lalthazuala Rokhum
rokhum@che.nits.ac.in

Specialty section:
This article was submitted to Heterogeneous Catalysis, a section of the journal Frontiers in Catalysis

Received: *07 April 2022*
Accepted: *12 May 2022*
Published: *08 June 2022*

Citation:
Kumawat MK and Rokhum SL (2022) Biodiesel Production From Oleic Acid Using Biomass-Derived Sulfonated Orange Peel Catalyst. Front. Catal. 2:914670. doi: 10.3389/fctls.2022.914670

1 INTRODUCTION

Worldwide, energy scarcity and pollution are seen as severe problems to human society. Energy consumption has risen drastically due to increased population growth and urbanization, as well as rapid industrialization. Fossil fuels provide us up to 88% of significant energy demand and 57.7% of transportation sector requirements (Naji and Tye, 2022). On the other hand, the depletion of fossil fuels encourages the search for alternative energy sources and clean fuel sources to ensure global energy security. As a result, many researchers are promoting the development of new alternative energy sources that have a low environmental impact (Sharma et al., 2020). In this perspective, biodiesel has received much attention in recent years as a possible alternative to diesel (Changmai et al., 2019). Biodiesel is made mostly from vegetable oils, animal fats, and waste cooking oil (WCO), and it has attractive properties such as non-toxicity, renewability and biodegradability (Laskar et al., 2018). It has similar physicochemical features such as petroleum-derived diesel and has a favourable combustion emission profile (Zhang et al., 2015). Furthermore, biodiesel can be utilised alone or in combination with petroleum diesel (da Luz Corrêa et al., 2020).

The high cost of raw ingredients (biodiesel feedstocks) is the most significant economic barrier in biodiesel production. Hence, non-edible vegetable oils such as Jatropha oil, Mahua oil, Karanja oil etc. are thus seen as attractive raw resources due to their lower cost, and also do not compete with food for human consumption (Bahar et al., 2020; Bastos et al., 2020). Because of product separation and wastewater treatment, homogeneous base and acid have strong catalytic capabilities in biodiesel production but poor environmental friendliness (Mazaheri et al., 2018; Zhang et al., 2019a). Heterogeneous catalysts provide several advantages over homogeneous catalysts, including the ability to be reused, easy separation, and environmental friendliness (Montefrio et al., 2010; Zhang et al., 2019b). The advantages of utilising heterogeneous rather than homogeneous catalysts for biodiesel production are essentially economic and practical (Tang et al., 2018). However, non-edible oil contains high free fatty acids (FFA), and moisture

content that might lead to soap formation as a side reaction while using an alkali catalyst (Wang et al., 2018; Seffati et al., 2019). For inedible feedstock oils with high FFA, prior deacidification of FFAs into alkyl esters of fatty acids (FAAEs) *via* esterification is required which often makes the whole synthesis complicated and time consuming (Sangar et al., 2019). In recent years, microwave assisted biodiesel synthesis is gaining momentum largely due to the rapid and homogeneous heating of the reaction mixture under microwave-radiation, thereby greatly improved the reaction rate and minimize the reaction time, hence economical (Khedri et al., 2019).

Owing to the requirement of acid catalysts for conversion of non-refined oil or inedible oil with high FFA to biodiesel, many researchers have reported a variety of heterogeneous acid catalysts, including sulfonic acid supported on SBA-15 (Zuo et al., 2013), tungstophosphoric acid incapacitated on zirconia (Alcañiz-Monge et al., 2018), sulfonated macro-porous cation exchange resins solid catalysts (Fu et al., 2015) etc. In recent years, biomass residue as a precursor of carbon-based solid acid catalyst has received a lot of interest owing to their abundant availability, biodegradability, low-cost and environmental friendly (Liu et al., 2010; Huang et al., 2018). Nonetheless, several acid functionalised biomass based material where prepared from cacao shell (Bureros et al., 2019), coconut coir husk (Thushari et al., 2019), bamboo (Zhou et al., 2016), Palm kernel shell (Farabi et al., 2019), and sugar bagasse (Ezebor et al., 2014).

Oranges (*Citrus sinensis*) are one of the most widely consumed fruits, globally. There is a high demand for oranges, which has resulted in the creation of vast quantities of orange peel (OP) waste. The majority of orange peels in China are dumped as waste, resulting in resource waste and environmental degradation (Pan et al., 2021). As a result, more study into alternative uses for orange peel waste is required. OP-derived carbon has previously been used to make supercapacitors (Wan et al., 2020), adsorbents (Safari et al., 2019), and fluorescent switching sensors (Wang et al., 2020). The synthesis of dihydropyrano [2,3-c] pyrazole derivatives *via* multi-component reactions was assisted by the use of OP-derived carbon powder mixed with sulfonic acid (Nagasundaram et al., 2020). Herein, we reported a "one-pot" synthesis of sulfonated carbon-based solid acid catalyst from OP, and used it for the microwave-assisted esterification of oleic acid as a model substrate to produce biodiesel.

2 MATERIALS AND METHODS

2.1 Materials

An orange peel was collected from a market in Mizoram (India). Sigma Aldrich supplied the oleic acid (OA, 99%). Merck provided MeOH (99.8%), $BaCl_2$ (99.95%), H_2SO_4 (98.06% purity, LR), NaOH (97.79%), and phenolphthalein (98%). All compounds were utilised as they were supplied without further purification. A Simplicity® UV Water Purification System was used to obtain deionized water (Merck).

2.2 Preparation of Catalyst

The OP was first to cut into strips and then dried under sunlight. The dried OP was pulverized into fine powder. Partial carbonization and sulfonation were used to make different OP-SO_3H catalysts by changing reaction time (18, 20, 22, 24 h), OP: H_2SO_4 ratio (1/5, 1/10, 1/15, and 1/20 g ml^{-1}) and temperature were varied between 80 and 120°C. **Table 1** listed the different catalysts synthesized by changing reaction time, temperature, OP:H_2SO_4 ratio, sulfur content, total acid density and biodiesel yield. In a typical experiment, OP (1 g) was dissolved entirely in H_2SO_4 (OP: H_2SO_4 ratios of 1/20 (g ml^{-1})) in a Pyrex bottle, and placed it in a hot air oven at 100°C for 18 h. After cooling to room temperature, the mixture was diluted with 50–60 ml deionized water, then washed with hot deionized water until no unreacted sulphate ions were found in the filtrate (using 6 mol L^{-1} $BaCl_2$ solution). The resulting black solid OP-SO_3H was dried for 12 h under vacuum at 80°C.

2.3 Catalyst Characterization

The modified Boehm titration method was used to estimate the densities of the –COOH, –SO_3H, and –OH groups on the OP-SO_3H surface (Rokhum et al., 2022). The combined –COOH/–SO_3H density and total acid density were determined using basic solutions. Total acid density and –COOH/-SO_3H density were determined using NaOH and $NaHCO_3$, respectively. 15 ml of 2 M NaCl solution was mixed in 50 mg catalyst and agitated thoroughly for 24 h. To titrate the filtered reaction mixture against a 0.02 M NaOH solution, the phenolphthalein indicator was used. Cu Kα radiation with 2θ = 10–60° was used for powdered X-ray diffraction (PXRD) on a PANalytical X'Pert Pro diffractometer. 40 kV and 100 mA were the operating voltage and current, respectively. The sample was degassed at 150°C for 10 h before being subjected to Brunauer-Emmet-Teller (BET) analysis on a Micromeritics ASAP 2010 surface area and porosity analyzer. A FEI-Quanta FEG 200F microscope was utilised for scanning electron microscopy (SEM) and energy-dispersive X-ray spectroscopy (EDS) at 80 mA beam current, 30 kV, and 60000 × magnification power. The catalyst was dispersed in ethanol and dropped onto an Au grid dropwise before being dried in an oven. On a PHI 5000 VersaProbe III apparatus with a micro-focused dual-anode Al/Mg K-source monochromated Al K X-ray sources and dual anode Al/Mg K-source, X-ray photoelectron spectroscopy (XPS) was performed. Thermogravimetric analysis (TGA) was conducted using a Metter Toledo TGA/DSC 1 in the temperature range of 25–650°C with a heating rate of 10°C min^{-1} under continuous flow of N_2.

2.4 Catalyst Activity and Reusability Test

In a 10 ml microwave tube, oleic acid (0.28 g, 1 mmol), methanol (0.48 g, 15 mmol), and catalyst (19.78 mg, 7 wt.% with regard to oleic acid) were added. The reaction mixture was then stirred at 600 rpm in a closed microwave reactor (Discover SP Microwave System) at 80°C and 50 W of power to afford the methyl oleate biodiesel (**Scheme 1**). Thin-layer chromatography was used to monitor the reaction's progress (TLC). At the end of the reaction, the catalyst was isolated from the reaction mixture using centrifugation (4,000 rpm, 7 min) and a rotary evaporator to remove excess methanol. Prior to reuse, the catalyst was washed with methanol (3 × 20 ml) and dried in vacuum oven at 80°C for 4 h. The production and purity of the biodiesel (FAME) product were confirmed by ^{1}H and ^{13}C NMR analysis.

2.5 Ester Characterization

^{1}H and ^{13}C NMR spectroscopy were used to investigate the purity and identity of the esterification product. A Bruker AVANCE spectrometer was used to conduct the tests.

$$Conversion\ (\%) = \frac{2A_{OMe}}{3A_{CH_2}} X100 \quad (1)$$

Here, A_{OMe} denotes the integration of the methoxy groups in FAME, and A_{CH_2} denotes the overall integration (OA + FAME) of -CH_2 in this equation **Eq. 1**.

2.6 Reaction Kinetics

Even though alcohols are commonly used in excess of the requisite stoichiometric molar ratio of 15:1(methanol to OA), esterification is usually thought to be a pseudo- first order process (Kaur and Ali, 2014). Reactions were carried out at four different temperatures to calculate the activation energy: 50, 60, 70, and 80°C. As a result, the reaction rate (r) could be written as:**Eq. 2**

$$r = -\frac{d[OA]}{dt} = k[OA] \quad (2)$$

Here, the rate constant is k, the concentration of oleic acid is [OA], and the reaction time is t. Monitoring methyl oleate conversion at varying t in **Eq. (3)** yielded first-order rate constants. The activation energy (E_a) (Wang et al., 2019a) was calculated using the Arrhenius equation (**Eq. 4**) and rate constants at various temperatures (50–80°C)

$$-\ln\ (1 - X) = kt \quad (3)$$

$$\ln k = -\frac{E_a}{RT} + \ln A \quad (4)$$

Here, X represents the oleic acid conversion at time t, T represents the reaction temperature, A represents the pre-exponential factor, and R is 8.314 $J.K^{-1}.mol^{-1}$.

3 RESULTS AND DISCUSSION

3.1 Sulfonation Parameters and the Composition of the Catalyst

The structure and morphology of the catalyst, active site characteristics, and sulfonic acid density are all influenced by the sulphonation temperature, time and OP to sulfuric acid ratio (g ml^{-1}) As shown in **Table 1** (Zhang et al., 2021). To assess the amount of sulfonation, four batches of OP-SO_3H catalysts with orange peel and conc. H_2SO_4 in the ratios of 1:5, 1:10, 1:15, and 1:20 (g ml^{-1}) were made in pyrex bottles with various reaction times ranging from 16 to 24 h at different temperatures ranging from 80 to 120°C. The sulfur (S) content and overall acidity were quite low in contrast to the other batches because the sulfuric acid supplied in the first batch (1:5) was quite low. In independent studies, the total acid densities diferrent OP-SO_3H catalyst prepared under different parameters as displayed in **Table 1**, were examined. From **Table 1**, it was observed that OP-SO_3H-4 catalyst with 'S' content of 4.73 has the highest total acidity (1.96 mmol g^{-1}) and afforded 96.51 ± 0.4% conversion of oleic acid to methyl oleate biodiesl and corresponding 96.03 ± 0.4% biodiesel yield under the optimized reaction conditions of 15:1

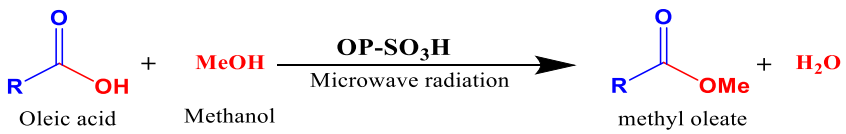

SCHEME 1 | OP-SO_3H as a heterogeneous catalyst for oleic acid esterification.

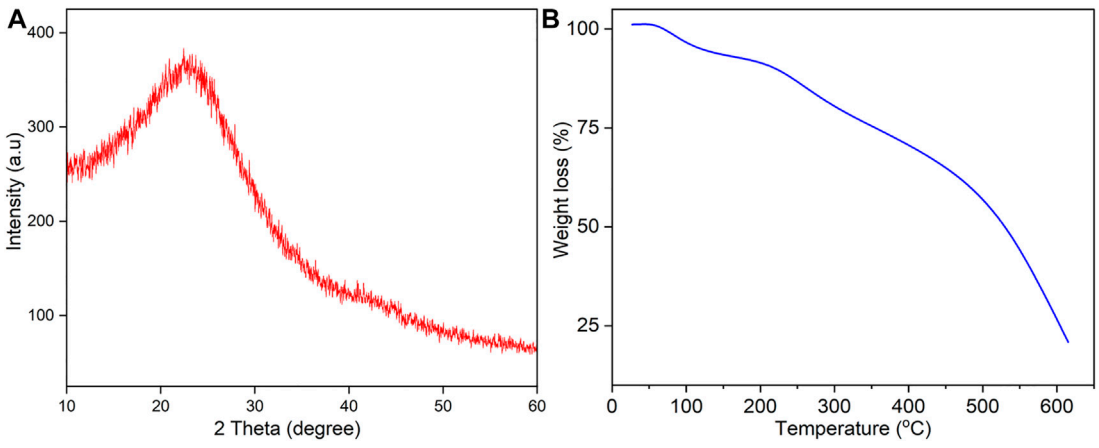

FIGURE 1 | (A) XRD pattern, **(B)** TGA thermogram.

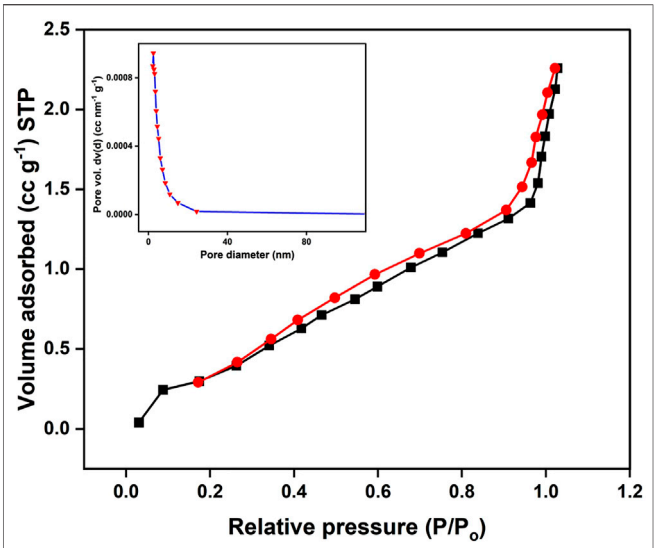

FIGURE 2 | N_2 adsorption-desorption isotherm and BJH pore size distribution curve (inset) for OP-SO_3H-4.

methano to OA ratio, 7 wt.% catalyst loading, 80°C temperature and a reaction time of 60 min. Nonetheless, on further increasing the sulfuric acid concentration (Entry 13, OP-SO_3H-13), there was a slight decrease in 'S' contents as well as total acidity, owing to the fact that when sulfuric acid concentrations are high, the -OH and -COOH groups are removed from the acid, decreasing the overall acidity of the solution (Anderson et al., 2014). With increasing dehydration, cyclization and aromatization occurs more rapidly, lowering the amount of surface that may be accessible for sulfonation as a result, reducing the quantity of S in the final product. Increased the period of sulfonation resulted in increasing acid densities of the catalysts until an optimum time of 24 h was attained. However, an increase in the sulfonation period beyond the optimum point had led to a slight decrease in total acid density values of the catalytic system (**Table 1**, entry 4 vs. entry 14). The 1:20 ratio exhibited the greatest sulphur content (4.73 wt.%) and total acid density (1.96 mmol g^{-1}) as shown in **Table 1**, Entry 4. Therefore, it was established that when sulfuric acid is supplied at a greater concentration during sulfonation, more –SO_3H groups may be attached to the catalyst surface, indicating that the process is more efficient (Gong et al., 2019; Parreño et al., 2020).

3.2 PXRD

The PXRD pattern of OP-SO_3H-4 sample is shown in **Figure 1A**. In OP-SO_3H-4 sample, a broad peak corresponding to C (0 0 2) plane diffraction at 2θ angles of 10°–30° was detected, which is attributable to non-graphitic carbon sheets orientated in a random way, while a faint diffraction peak from 40° to 50° is related to the presence of crystalline graphite (Pan et al., 2021). The observed PXRD pattern is similar to our previous report of amorphous glucose derived sulfonic acid catalyst (Rokhum et al., 2022).

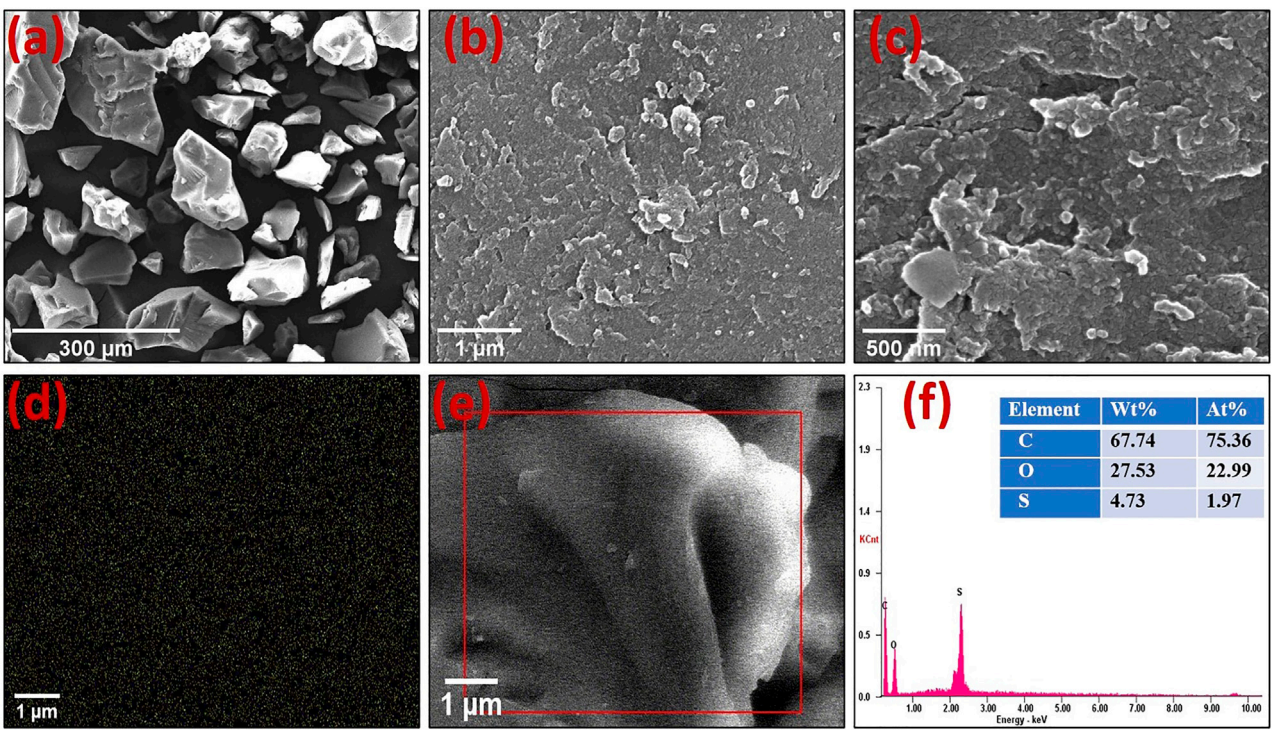

FIGURE 3 | Representative SEM images of catalyst OP-SO_3H-4 at various magnifications **(A–C)**. EDS mapping of Sulfur **(D)**, SEM images from where elemental mapping was analyzed, and SEM-EDS elemental mapping **(F)** of the area in the red box in **(E)**.

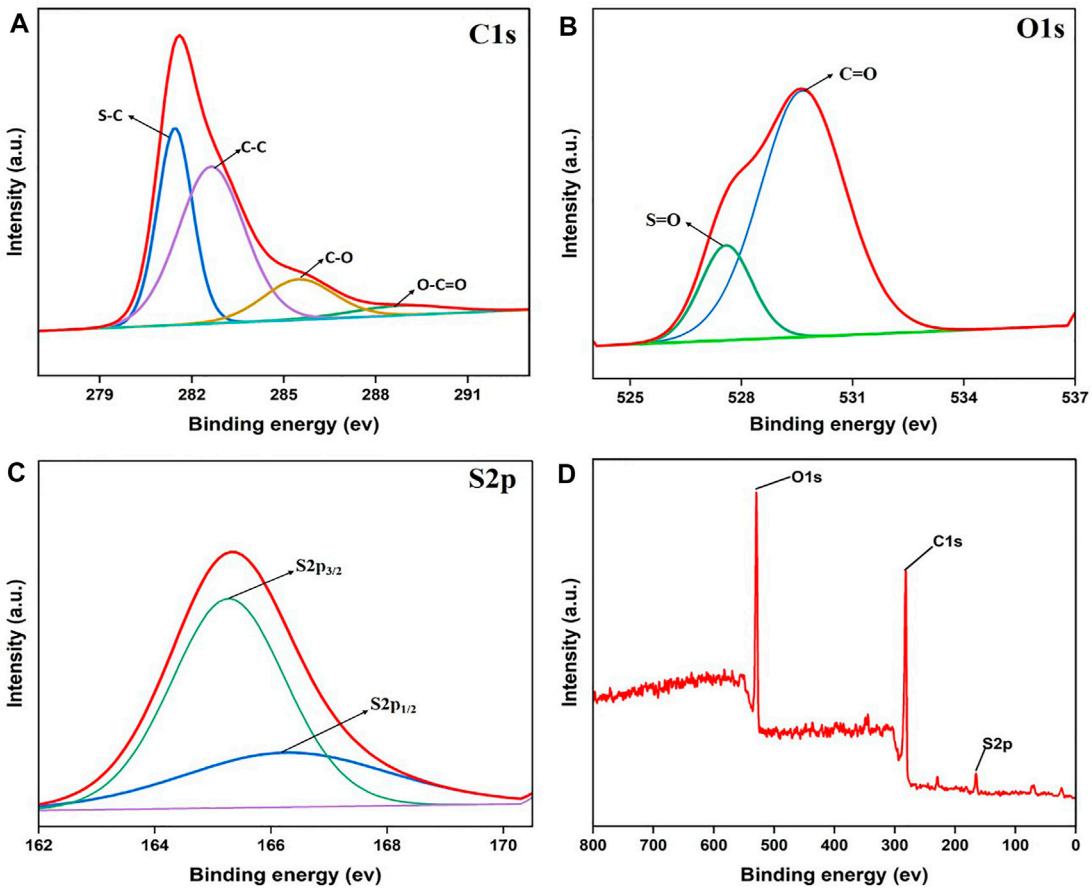

FIGURE 4 | The deconvolution of the XPS spectra of OP-SO_3H-4. **(A)** Carbon, **(B)** Oxygen. **(C)** Sulfur, **(D)** Overall XPS spectrum.

TABLE 1 | Catalysts were produced under various sulfonation circumstances and observed acid densities.

Sr. No.	Sample	OP/S[a]	T (h)	T (°C)	Sulfur content	Total acid density (mmol g^{-1})	Biodiesel yield (%)[b]
1	OP-SO_3H-1	1:5	24	100	2.07	0.64	58.24
2	OP-SO_3H-2	1:20	24	80	2.39	0.86	73.59
3	OP-SO_3H-3	1:15	24	100	4.02	1.37	87.38
4	OP-SO_3H-4	1:20	24	100	4.73	1.96	96.03
5	OP-SO_3H-5	1:10	24	100	2.18	0.72	64.81
6	OP-SO_3H-6	1:20	24	120	3.99	1.36	87.16
7	OP-SO_3H-7	1:15	18	100	3.51	1.06	81.23
8	OP-SO_3H-8	1:20	18	100	2.27	0.81	71.75
9	OP-SO_3H-9	1:15	20	100	4.01	1.38	87.47
10	OP-SO_3H-10	1:20	20	100	4.29	1.52	88.91
11	OP-SO_3H-11	1:15	22	100	4.17	1.44	88.14
12	OP-SO_3H-12	1:20	22	100	4.51	1.69	92.54
13	OP-SO3H-13	1:25	24	100	4.57	1.73	92.95
14	OP-SO3H-14	1:20	28	100	4.61	1.84	93.68

[a]*OP (g): Sulfuric acid (g) ratio.*
[b]*Methanol to OA molar ratio, catalyst loading (wt.%), temperature (°C), time (min).*

3.3 TGA

The TGA curve of the OP-SO_3H-4 catalyst is shown in **Figure 1B**. TGA analysis was used to determine the decomposition pattern of the OP-SO_3H-4 catalyst. Initial weight loss was seen up to 100°C temperature due to adsorbed moisture on the OP-SO_3H-4 catalyst. The decomposition of single bond -SO_3H, single bond -COOH

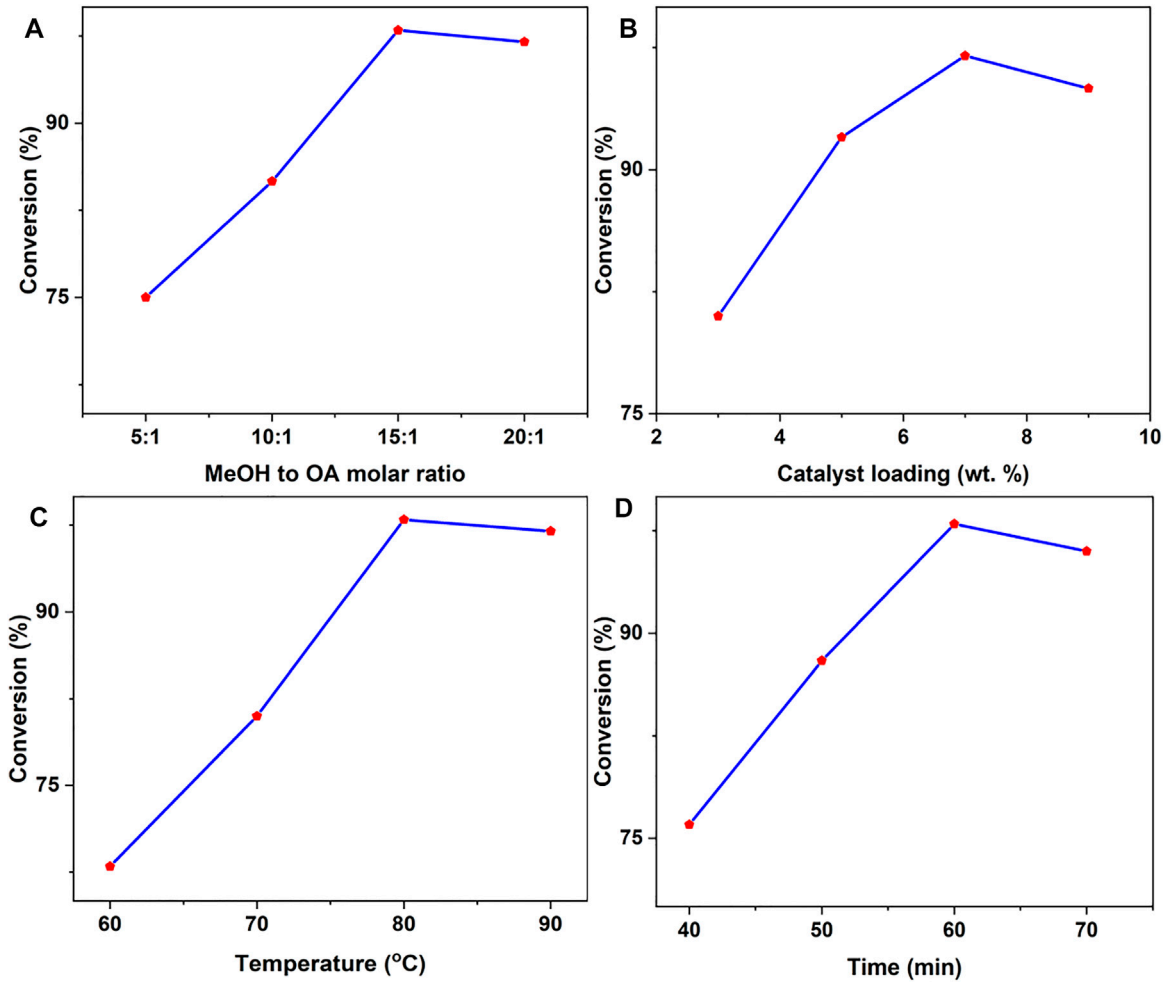

FIGURE 5 | Effects of various factors on oleic acid esterification. **(A)** Varying the methanol to OA molar ratio from 5:1 to 20:1 (other conditions: 7 wt.% catalyst loading, 80°C reaction temperature, 60 min reaction time). **(B)** Changing the catalyst loading from 3 to 9 wt.% relative to OA (other conditions: MeOH to OA molar ratio 15:1, 80°C reaction temperature, 60 min reaction time). **(C)** Temperatures ranging from 60 to 90°C (other conditions: MeOH to OA molar ratio 15:1, 7 wt.% catalyst loading, 60 min reaction time). **(D)** Changing the time from 40 to 75 min (alternative conditions: MeOH to OA molar ratio 15:1, 7 wt.% catalyst loading, 80°C reaction temperature).

TABLE 2 | Textural properties of OP-SO_3H-4.

Sr. No.	Properties	OP-SO_3H-4
1	Surface area	3.617 m^2 g^{-1}
2	Pore volume	0.004 cc g^{-1}
3	Average pore size	2.467 nm

groups, single bond -OH group and the little quantity of carbon support may cause a second weight loss between 180 and 390°C. Up to 600°C, the whole weight loss occurred, and the remaining part exists as graphene-like carbon bodies (Lathiya et al., 2018).

3.4 BET

Figure 2 illustrates the nitrogen adsorption–desorption isotherms of the OP-SO_3H-4 sample. The sample's isotherms have type-IV characteristics. **Table 2** lists the microstructure characteristics of the OP-SO_3H-4 sample. Moreover, using the BET and BJH technique, the specific surface areas, pore volume and average pore size of the catalysts are determined to be 3.617 m^2 g^{-1}, 0.004 cc g^{-1}, and 2.467 nm, respectively.

3.5 SEM Images and EDS

SEM pictures at various magnifications have been used to reveal the surface structure of the OP-SO_3H-4 catalyst (**Figure 3**). As previously reported, certain cracks appeared on the surfaces of the OP-SO_3H-4 catalyst, which were ascribed to partial oxidation, partial degradation, and condensation of the porous structure during sulfonation (Lathiya et al., 2018). The sample had a regular composition, showing plenty of C, O, and S, according to EDS results (**Figure 3F**). 4.73 wt.% S (1.96 mmol g^{-1}) was present, according to EDS data.

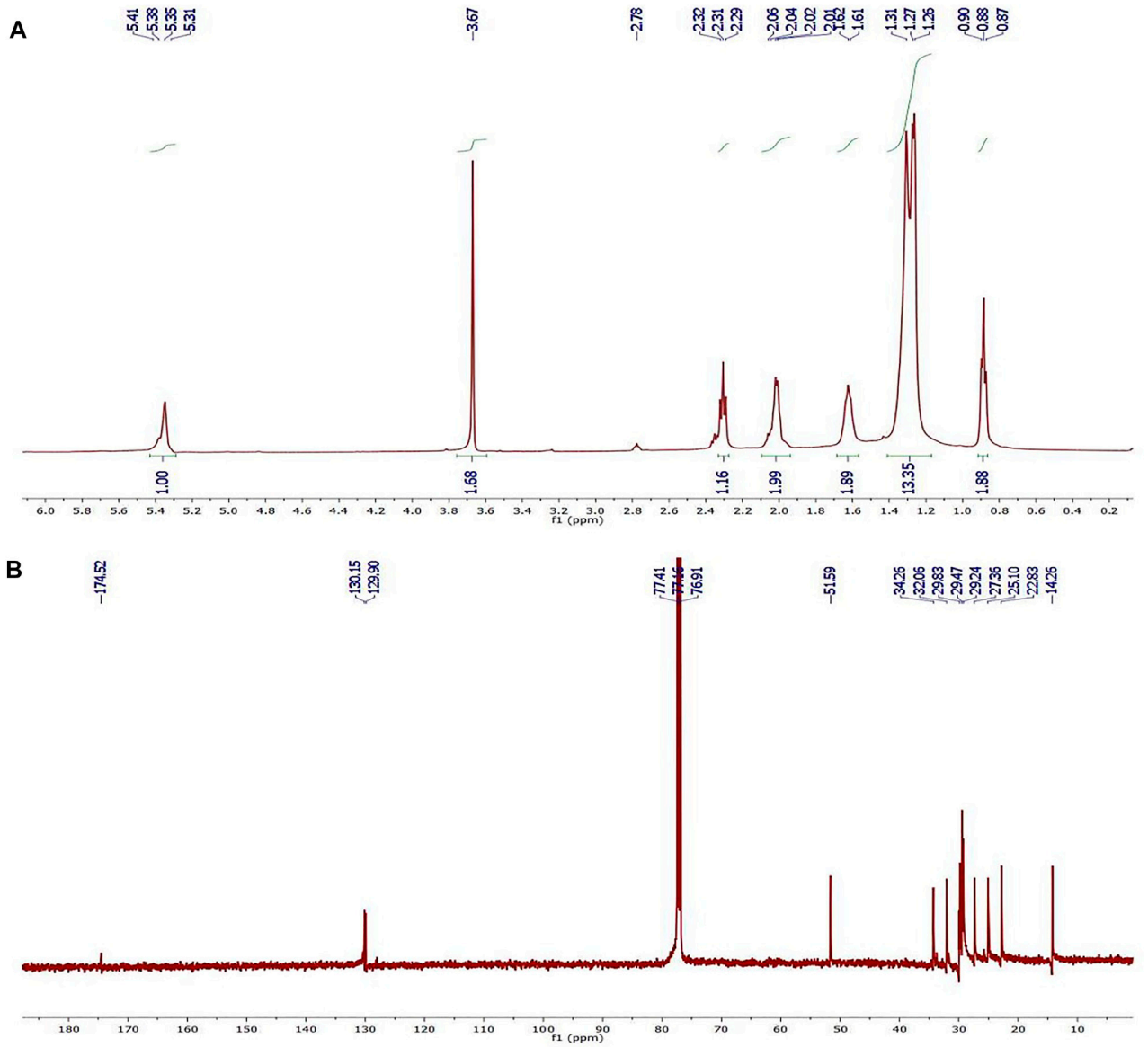

FIGURE 6 | (A) ^{1}H NMR (500 MHz, 28°C, $CDCl_3$) and **(B)** ^{13}C NMR (175 MHz, 28°C, $CDCl_3$) spectra of methyl oleate. (optimized conditions: 15:1 MeOH to OA molar ratio, 7 wt.% catalyst loading, 60 min reaction time and 80°C reaction temperature).

3.6 XPS

The surface composition of the produced OP-SO_3H-4 catalyst was examined using X-ray photoelectron spectroscopy (XPS). The deconvoluted peaks for the elements of Oxygen (O1s), Carbon (C1s), and Sulfur (S2p) on the OP-SO_3H-4 catalyst surface are shown in **Figure 4**. As shown in **Figure 4A**, the C1s spectrum has been deconvoluted into four peaks with binding energies of 281.44 eV for C-S, 283.64 eV for C-C, 286.41 eV for C-O, and 289.07 eV for O-C=O. It is possible to distinguish two peaks associated to the O1s spectrum (**Figure 4B**), which correspond to S=O at 528.16 eV, C=O at 531.57 eV, respectively. Two components of the deconvoluted S2p band were identified in **Figure 4C**, where $S2p_{3/2}$ (165.27 eV) and $S2p_{1/2}$ (166.56 eV) are ascribed to characteristic peak of SO_3H. According to **Figure 4D**, the overall binding energy of some elements in OP-SO_3H-4 may be determined. The observed data is similar to the reported XPS given by Nagasundaram et al. (Nagasundaram et al., 2020).

3.7 Optimization of Conversion of Oleic Acid to Biodiesel

Following its characterization, the potential use of a sulfonic acid functionalized orange peel catalyst was investigated in the production of biodiesel by esterification of OA using the catalyst. Optimizing approaches were used to establish the

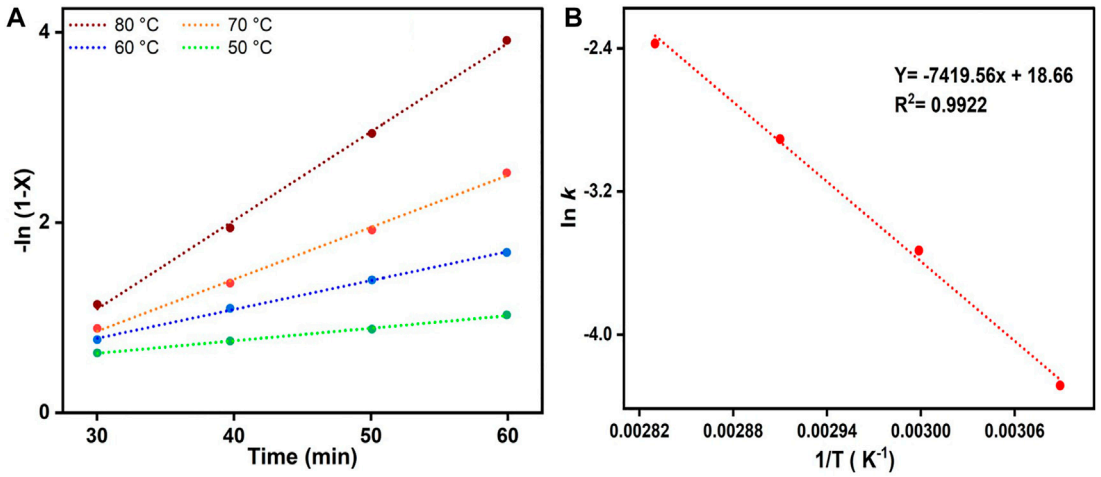

FIGURE 7 | (A) Graphical representation of –ln (1–X) vs. t (where, X is conversion of OA) at different temperatures for the esterification of oleic acid with MeOH. **(B)** The corresponding Arrhenius plot of ln k vs. 1/T.

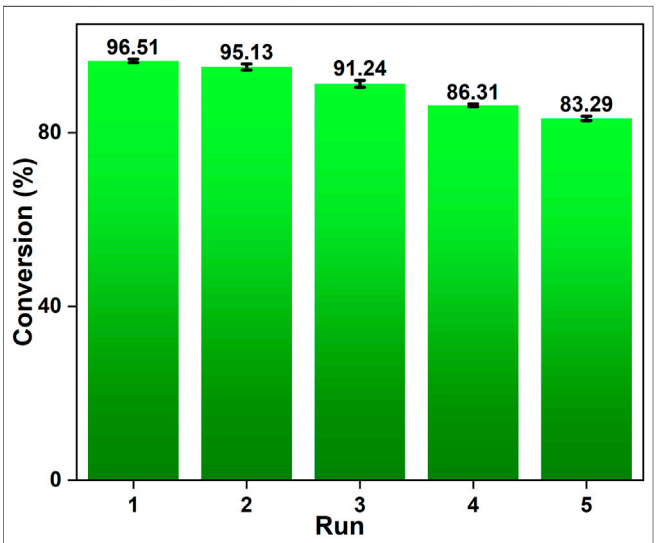

FIGURE 8 | Graphical representation of OP-SO_3H-4 reusability in the esterification of oleic acid during 5 cycles (columns 1–5).

exact reaction conditions for biodiesel production. The influence of catalyst wt.%, methanol to oleic acid molar ratio, temperature, and time on the reaction was explored in detail.

The findings were obtained using a very acidic catalyst, OP-SO_3H-4 (with the maximum total acid density of 1.96 mmol g^{-1} and the highest S concentration of 4.73 wt.%). A representation of the ^{1}H and ^{13}C NMR spectrum of the product obtained from catalytic testing (MeOH to OA molar ratio 15:1, 7 wt.% catalyst loading, 60 min at 80°C reaction temperature; see below for details on the optimization of the reaction conditions) is shown in **Figure 5**. For OA and methyl oleate, triplet integration at δ 2.32 and δ 2.29 ppm, respectively, found 96.51 ± 0.4% esterification (Sanjay, 2013).

3.7.1 Effect of Methanol to OA Molar Ratio

The effect of the methanol to OA molar ratio on the esterification reaction in **Figure 5A** was examined by adjusting the ratio from 5:1 to 20:1 while employing a 7 wt.% loading of OP-SO_3H-4 catalyst at 80°C reaction temperature for 60 min reaction time. Excess methanol drove the equilibrium forward, as expected when the molar ratio was increased. At a 15:1 methanol to OA ratio, the maximum OA conversion (96.51 ± 0.4%) was achieved. However, as more methanol was added to the reaction mixture, it diluted the reaction mixture and potentially allowed more water into the system, which would promote the reverse reaction (Zhang et al., 2014).

3.7.2 Effect of Catalyst Loading

Using the optimal 15:1 methanol to OA molar ratio at 80°C reaction temperature for 60 min reaction time, catalyst loading was adjusted from 3 to 9 wt.% (**Figure 5B**). As expected, OA conversion improved with catalyst quantity, reaching the highest of 96.51 ± 0.4% at 7 wt.%, before declining marginally (to 95.86 ± 0.6%) at 9 wt.%. If significant, this decline would be in accordance with previous observations that mentioned product adsorption/blockage of active centers as well as increased viscosity of the reaction mixture as factors limiting mass transfer (Mutreja et al., 2014).

3.7.3 Effect of Temperature

The temperature was varied between 60 and 90°C, under the reaction condition of methanol to OA molar ratio 15:1, 7 wt.% catalyst loading, 60 min reaction time in a closed vessel under microwave irradiation (50 W) with a working pressure of 100 psi/6.8 bar (**Figure 5C**). Since the esterification of OA with a solid catalyst is a three-phase system (methanol-catalyst-OA), temperature control of reagent access to active sites is crucial. As expected for an endothermic process, when the temperature was raised, the conversion increased (Thinnakorn and Tscheikuna, 2014). Acid conversion declined at 90°C, which was attributed to methanol evaporation.

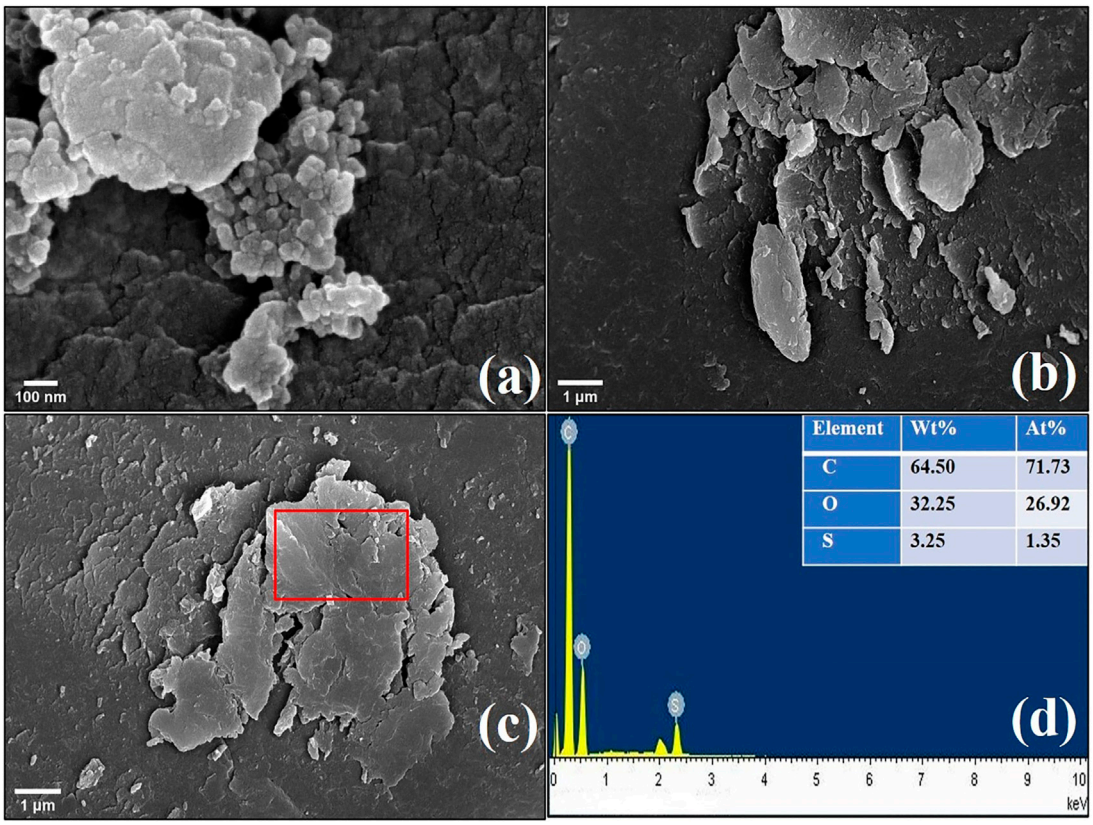

FIGURE 9 | Representative SEM image at different magnification of recovered catalyst after the 5th cycle **(A,B)**. EDS spectrum **(D)** of the region in the red box in **(C)**.

TABLE 3 | For the conversion of OA to biodiesel, the current catalyst was compared to a previously described catalyst.

Sr. No.	Catalyst	Conditions[a]	TOF (mol g^{-1} h^{-1})	Conversion (%)	Ref.
1	C-SO_3H	16:1, 17, 95, 4	0.005	99.9	Hara, (2010)
2	FSS-IL[b]	10:1, 10, 100, 4	0.008	93.5	Wan et al. (2015)
3	Sulfonated ginger straw	9:1, 7, 64, 3.5	0.013	93.2	Yu et al. (2021)
4	$Zr_{1.0}Fe_{1.5}$-SA-SO_3H	12:1, 9, 90, 5	0.007	96.6	Wang et al. (2019b)
5	Fe_3O_4@ZIF-8/TiO_2[c]	30:1, 6, 50, 1.25	0.043	93	Moatamed Sabzevar et al. (2021)
6	TiO_2(10)/NP[d]	8:1, 10, 150, 8	0.003	87	Essamlali et al. (2017)
7	Sulfonated Sargassum horneri carbon	15:1, 10, 70, 3	0.011	96.4	Cao et al. (2021)
8	SO_3H-HM-ZSM-5-3	18:1, 5.2, 88, 10	0.006	92.45	Mostafa Marzouk et al. (2021)
9	Biochar	30:1, 5, 315, 3	0.011	48	Dehkhoda and Ellis, (2013)
10	E-P400-2-SO_3H[e]	15:1, 5, 80, 5	0.013	96.5	Huang et al. (2016)
11	OP-SO_3H-4	15:1, 7, 80, 1[f]	0.049	96.51 ± 0.4	This work

[a]*Methanol to OA molar ratio, catalyst loading (wt.%), temperature (°C), time (h).*
[b]*FSS-IL = Fe_3O_4@SiO_2@meso-SiO_2-ionic liquid.*
[c]*ZIF-8 = zeolitic imidazolate framework-8.*
[d]*TiO_2(10)/NP = Natural phosphate-supported titania.*
[e]*E-P400 = lignin carbonized in sub-critical EtOH.*
[f]*Microwave irradiation.*

3.7.4 Effect of Time

The catalyst dosage of 7 wt.% at 80°C reaction temperature and methanol to OA molar ratio of 15:1, a reaction duration of 24–96 min under microwave irradiation was investigated. Due to mass transfer constraints in the heterogeneous system (Pan et al., 2016), the biodiesel yield is only 77.32 ± 0.5% at 24 min, as shown in **Figure 5D**. After that, the yield increased to 96.03 ± 0.4% (corresponding to 96.51 ± 0.4% conversion of oleic acid to biodiesel) in 60 min before declining.

The ^{1}H NMR spectrum of methyl oleate biodiesel is shown in **Figure 6A**. The -CH_2 protons are represented as a triplet signal at 2.31 ppm. The presence of methoxy protons as singlet at 3.67 ppm confirms the formation of methyl oleate biodiesel. Among the signals observed were a triplet signal of 0.88 ppm from the terminal methyl protons, a strong quartet signal of 1.27 ppm from the carbon chain's methylene protons, a singlet signal of 1.61 ppm from the β-carbonyl methylene protons, and another of 5.38 ppm from the terminal olefinic hydrogen (Mello et al., 2008; Tariq et al., 2011).

The ^{13}C NMR spectrum of methyl oleate is shown in **Figure 6B**. The signal at 174.52 ppm corresponds to the carbonyl carbon of the ester molecules, while the signal at 130.15 ppm corresponds to the olefinic carbons of the esters. When analyzing the ^{13}C NMR spectra of biodiesel, the signal at 51.59 ppm is due to the presence of methyl esters' methoxy carbons. The methylene and methyl carbons of the fatty acid moiety are present in concentrations ranging from 14.26 to 34.26 ppm (Basumatary et al., 2013).

3.8 Kinetics Study of Oleic Acid Esterification

The graph in demonstrated a linear connection between -ln (1-X) and time for reactions carried out at temperatures ranging from 50 to 80°C, validating our assumption that esterification follows pseudo-first-order kinetics (**Figure 7A**). It was possible to calculate the activation energy (Ea) of the esterification process by inserting the rate constants in the Arrhenius equation (**Eq. 3**). On the basis of the ln k versus T^{-1} figure, pseudo-first-order kinetics may be constructed. The pre-exponential component and Ea for the reaction may be calculated from the intercept and slope (-Ea/R) of the line (Changmai et al., 2021). The pre-exponential factor in the present study was calculated to be 1.27×10^{8} min^{-1}. Ea was calculated from **Figure 7B** and was found to be 61.68 kJ mol^{-1}, which is within the range of 33–84 kJ mol^{-1}. This is standard for esterification, and it demonstrates that the present catalyst causes a very significant drop in activation energy when compared to a range of different esterification catalysts (Putra et al., 2018).

3.9 Catalyst Reusability

Reusability of the catalyst is critical for industrial applications from an economical perspective. A good solid catalyst must keep the exceptional quality of a high catalytic activity after repeated usage in addition to having a comparatively high catalytic efficiency. As a result, we investigated the reusability of the OP-SO_3H-4 catalyst. We were able to perform 5 reaction cycles with the OP-SO_3H-4 using the optimal reaction parameters (15:1 methanol to OA molar ratio, 7 wt.% catalyst loading, 80°C reaction temperature, 60 min reaction time). The catalyst was collected from the reaction mixture and washed with methanol (3 × 20 ml) after each cycle of reaction. The recovered catalyst was then dried in a vacuum oven at 80°C for 4 h. The conversion of OA to its equivalent methyl oleate declined slightly with each subsequent reaction cycle yielding 83.29 ± 0.5% for the 5th cycle (**Figure 8**). According to prior knowledge, leaching of sulphur (Azargohar and Dalai, 2008; Chen et al., 2016), and methylation of sulfonic acid groups (Chen et al., 2016) were primarily responsible for the decline in oleic conversion in each reaction cycle. The SEM-EDS analysis of the recovered catalyst revealed that the sulphur concentration decreased from 4.73 wt.% (1.96 mmol g^{-1}) of fresh OP-SO_3H-4 (**Figure 3**) to 3.25 wt.% (0.99 mmol g^{-1}) of recovered catalyst (**Figure 9**). From SEM analysis images, no prominent changes were observed in the morphology of the recovered catalyst compare to fresh catalyst (**Figures 3** vs. **Figure 9**).

3.10 Comparison of the Current Catalyst With Previously Reported Catalyst

We summarized the catalytic performances of several acid functionalized solid catalysts using mainly conventional heating method (**Table 3**, Entry 1-10). The majority of them (except entry 9) have showed good OA to biodiesel conversion, but compared to OP-SO_3H-4, the other catalysts have some drawbacks, including longer reaction times (entries 1–4, 6-10), increased temperatures (entries 1-2, 4, 6, 8-9), high catalyst loading (entries 1–2, 4, 6-7) and high methanol to OA molar ratio (entries 1, 5, 8-9). As can be observed, the majority of reported catalysts had a lower turnover frequency (TOF) than OP-SO_3H-4, which had a TOF of 0.049 mol g^{-1} h^{-1}. Overall, it can be concluded that microwave irradiation greatly enhanced the speed of reaction due to rapid and homogenous heating unlike conventional heating method, thereby reducing the reaction time.

4 CONCLUSION

This study explored the microwave-assisted production of high-quality biodiesel–fuel from OA using OP-SO_3H-4 as the catalyst. By using microwave irradiation, the OP-SO_3H-4 was demonstrated to be an effective catalyst for generating environmentally friendly biodiesel–fuel. Using a lower catalyst quantity (7 wt.% of OA) and lower methanol to OA molar ratio (15:1) in a comparatively shorter reaction time (60 min) at 80°C, a conversion yield of 96.51 ± 0.4% was achieved. It was found that after five catalytic cycles, the catalyst retained its good stability and activity with no significant loss of activity. On the fifth catalytic cycle, a high conversion of 83.29 ± 0.5% methyl oleate biodiesel was recorded. It was determined that the leaching of sulphur from 4.73 wt.% (fresh) to 3.25 wt.% (5^{th} recycled) was the primary cause of the decline in conversion. SEM-EDS analysis confirmed this. Consequently, when compared to several synthetic catalysts, which are often toxic, unsustainable, costly, and non-biodegradable, the present catalyst has a significant influence on environmental preservation.

DATA AVAILABILITY STATEMENT

The original contributions presented in the study are included in the article/Supplementary Material, further inquiries can be directed to the corresponding author.

AUTHOR CONTRIBUTIONS

MK: Conceptualization, Methodology, Investigation, data curation, manuscript writing, SR: Supervision, Reviewing and Editing.

ACKNOWLEDGMENTS

We thank IIT Madras, IIT Indore, IIT Roorkee and IIT Bombay for the analysis.

REFERENCES

Alcañiz-Monge, J., Bakkali, B. E., El, Trautwein, G., and Trautwein, S. (2018). Zirconia-supported Tungstophosphoric Heteropolyacid as Heterogeneous Acid Catalyst for Biodiesel Production. *Appl. Catal. B Environ.* 224, 194–203. doi:10.1016/j.apcatb.2017.10.066

Anderson, J. M., Johnson, R. L., Schmidt-Rohr, K., and Shanks, B. H. (2014). Solid State NMR Study of Chemical Structure and Hydrothermal Deactivation of Moderate-Temperature Carbon Materials with Acidic SO3H Sites. *Carbon* 74, 333–345. doi:10.1016/j.carbon.2014.03.041

Azargohar, R., and Dalai, A. K. (2008). Steam and KOH Activation of Biochar: Experimental and Modeling Studies. *Microporous Mesoporous Mater.* 110, 413–421. doi:10.1016/j.micromeso.2007.06.047

Bastos, R. R. C., da Luz Correa, A. P., da Luz, P. T. S., da Rocha Filho, G. N., Zamian, J. R., and da Conceição, L. R. V. (2020). Optimization of Biodiesel Production Using Sulfonated Carbon-Based Catalyst from an Amazon Agro-Industrial Waste. *Energy Convers. Manag.* 205, 112457. doi:10.1016/j.enconman.2019.112457

Basumatary, S., Barua, P., and Deka, D. C. (2013). Identification of Chemical Composition of Biodiesel from Tabernaemontana Divaricata Seed Oil. *J. Chem. Pharm. Res.* 5, 172–179.

Bureros, G. M. A., Tanjay, A. A., Cuizon, D. E. S., Go, A. W., Cabatingan, L. K., Agapay, R. C., et al. (2019). Cacao Shell-Derived Solid Acid Catalyst for Esterification of Oleic Acid with Methanol. *Renew. Energy* 138, 489–501. doi:10.1016/j.renene.2019.01.082

Cao, M., Peng, L., Xie, Q., Xing, K., Lu, M., and Ji, J. (2021). Sulfonated Sargassum Horneri Carbon as Solid Acid Catalyst to Produce Biodiesel via Esterification. *Bioresour. Technol.* 324, 124614. doi:10.1016/j.biortech.2020.124614

Changmai, B., Rano, R., Vanlalveni, C., and Rokhum, L. (2021). A Novel Citrus Sinensis Peel Ash Coated Magnetic Nanoparticles as an Easily Recoverable Solid Catalyst for Biodiesel Production. *Fuel* 286, 119447. doi:10.1016/j.fuel.2020.119447

Changmai, B., Sudarsanam, P., and Rokhum, L. (2019). Industrial Crops & Products Biodiesel Production Using a Renewable Mesoporous Solid Catalyst. *Ind. Crop. Prod.* 111911. doi:10.1016/j.indcrop.2019.111911

Chen, W., Zhang, Q., Uetani, K., Li, Q., Lu, P., Cao, J., et al. (2016). Sustainable Carbon Aerogels Derived from Nanofibrillated Cellulose as High-Performance Absorption Materials. *Adv. Mat. Interfaces* 3, 1–9. doi:10.1002/admi.201600004

da Luz Correa, A. P., Bastos, R. R. C., Rocha Filho, G. N. d., Zamian, J. R., and Conceição, L. R. V. d. (2020). Preparation of Sulfonated Carbon-Based Catalysts from Murumuru Kernel Shell and Their Performance in the Esterification Reaction. *RSC Adv.* 10, 20245–20256. doi:10.1039/d0ra03217d

Dehkhoda, A. M., and Ellis, N. (2013). Biochar-based Catalyst for Simultaneous Reactions of Esterification and Transesterification. *Catal. Today* 207, 86–92. doi:10.1016/j.cattod.2012.05.034

Essamlali, Y., Larzek, M., Essaid, B., and Zahouily, M. (2017). Natural Phosphate Supported Titania as a Novel Solid Acid Catalyst for Oleic Acid Esterification. *Ind. Eng. Chem. Res.* 56, 5821–5832. doi:10.1021/acs.iecr.7b00607

Ezebor, F., Khairuddean, M., Abdullah, A. Z., and Boey, P. L. (2014). Esterification of Oily-FFA and Transesterification of High FFA Waste Oils Using Novel Palm Trunk and Bagasse-Derived Catalysts. *Energy Convers. Manag.* 88, 1143–1150. doi:10.1016/j.enconman.2014.04.062

Farabi, M. S. A., Ibrahim, M. L., Rashid, U., and Taufiq-Yap, Y. H. (2019). Esterification of Palm Fatty Acid Distillate Using Sulfonated Carbon-Based Catalyst Derived from Palm Kernel Shell and Bamboo. *Energy Convers. Manag.* 181, 562–570. doi:10.1016/j.enconman.2018.12.033

Fu, J., Cai, Z., Gong, Y., O'Reilly, S. E., Hao, X., and Zhao, D. (2015). A New Technique for Determining Critical Micelle Concentrations of Surfactants and Oil Dispersants via UV Absorbance of Pyrene. Colloids Surfaces A Physicochem. *Eng. Asp.* 484, 1–8. doi:10.1016/j.colsurfa.2015.07.039

Gong, R., Ma, Z., Wang, X., Han, Y., Guo, Y., Sun, G., et al. (2019). Sulfonic-acid-functionalized Carbon Fiber from Waste Newspaper as a Recyclable Carbon Based Solid Acid Catalyst for the Hydrolysis of Cellulose. *RSC Adv.* 9, 28902–28907. doi:10.1039/c9ra04568f

Hara, M. (2010). Biodiesel Production by Amorphous Carbon Bearing SO3H, COOH and Phenolic OH Groups, a Solid Brønsted Acid Catalyst. *Top. Catal.* 53, 805–810. doi:10.1007/s11244-010-9458-z

Huang, F., Li, W., Zhang, T., Li, D., Liu, Q., Zhu, X., et al. (2018). Conversion of Biomass-Derived Carbohydrates into 5-hydroxymethylfurfural Catalyzed by Sulfonic Acid-Functionalized Carbon Material with High Strong-Acid Density in γ-valerolactone. *Res. Chem. Intermed.* 44, 5439–5453. doi:10.1007/s11164-018-3432-y

Huang, M., Luo, J., Fang, Z., and Li, H. (2016). Biodiesel Production Catalyzed by Highly Acidic Carbonaceous Catalysts Synthesized via Carbonizing Lignin in Sub- and Super-critical Ethanol. *Appl. Catal. B Environ.* 190, 103–114. doi:10.1016/j.apcatb.2016.02.069

Kaur, N., and Ali, A. (2014). Kinetics and Reusability of Zr/CaO as Heterogeneous Catalyst for the Ethanolysis and Methanolysis of Jatropha Crucas Oil. *Fuel Process. Technol.* 119, 173–184. doi:10.1016/j.fuproc.2013.11.002

Khedri, B., Mostafaei, M., and Safieddin Ardebili, S. M. (2019). A Review on Microwave-Assisted Biodiesel Production. Energy Sources, Part A Recover. *Util. Environ. Eff.* 41, 2377–2395. doi:10.1080/15567036.2018.1563246

Laskar, I. B., Gupta, R., Chatterjee, S., and Vanlalveni, C. (2020). Taming Waste : Waste Mangifera Indica Peel as a Sustainable Catalyst for Biodiesel Production at Room Temperature. *Renew. Energy* 161, 207–220. doi:10.1016/j.renene.2020.07.061

Laskar, I. B., Rajkumari, K., Gupta, R., Chatterjee, S., Paul, B., and Rokhum, L. (2018). Waste Snail Shell Derived Heterogeneous Catalyst for Biodiesel Production by the Transesterification of Soybean Oil. *RSC Adv.* 8, 20131–20142. doi:10.1039/c8ra02397b

Lathiya, D. R., Bhatt, D. V., and Maheria, K. C. (2018). Synthesis of Sulfonated Carbon Catalyst from Waste Orange Peel for Cost Effective Biodiesel Production. *Bioresour. Technol. Rep.* 2, 69–76. doi:10.1016/j.biteb.2018.04.007

Liu, X. Y., Huang, M., Ma, H. L., Zhang, Z. Q., Gao, J. M., Zhu, Y. L., et al. (2010). Preparation of a Carbon-Based Solid Acid Catalyst by Sulfonating Activated Carbon in a Chemical Reduction Process. *Molecules* 15, 7188–7196. doi:10.3390/molecules15107188

Mazaheri, H., Ong, H. C., Masjuki, H. H., Amini, Z., Harrison, M. D., Wang, C. T., et al. (2018). Rice Bran Oil Based Biodiesel Production Using Calcium Oxide Catalyst Derived from Chicoreus Brunneus Shell. *Energy* 144, 10–19. doi:10.1016/j.energy.2017.11.073

Mello, V. M., Oliveira, F. C. C., Fraga, W. G., Do Nascimento, C. J., and Suareza, P. A. Z. (2008). Determination of the Content of Fatty Acid Methyl Esters (FAME) in Biodiesel Samples Obtained by Esterification Using 1H-NMR Spectroscopy. *Magn. Reson. Chem.* 46, 1051–1054. doi:10.1002/mrc.2282

Moatamed Sabzevar, A., Ghahramaninezhad, M., and Niknam Shahrak, M. (2021). Enhanced Biodiesel Production from Oleic Acid Using TiO2-Decorated Magnetic ZIF-8 Nanocomposite Catalyst and its Utilization for Used Frying Oil Conversion to Valuable Product. *Fuel* 288, 119586. doi:10.1016/j.fuel.2020.119586

Montefrio, M. J., Xinwen, T., and Obbard, J. P. (2010). Recovery and Pre-treatment of Fats, Oil and Grease from Grease Interceptors for Biodiesel Production. *Appl. Energy* 87, 3155–3161. doi:10.1016/j.apenergy.2010.04.011

Mostafa Marzouk, N., Abo El Naga, A. O., Younis, S. A., Shaban, S. A., El Torgoman, A. M., and El Kady, F. Y. (2021). Process Optimization of Biodiesel Production via Esterification of Oleic Acid Using Sulfonated Hierarchical Mesoporous ZSM-5 as an Efficient Heterogeneous Catalyst. *J. Environ. Chem. Eng.* 9, 105035. doi:10.1016/j.jece.2021.105035

Mutreja, V., Singh, S., and Ali, A. (2014). Potassium Impregnated Nanocrystalline Mixed Oxides of La and Mg as Heterogeneous Catalysts for Transesterification. *Renew. Energy* 62, 226–233. doi:10.1016/j.renene.2013.07.015

Nagasundaram, N., Kokila, M., Sivaguru, P., Santhosh, R., and Lalitha, A. (2020). SO3H@carbon Powder Derived from Waste Orange Peel: An Efficient, Nano-

Sized Greener Catalyst for the Synthesis of Dihydropyrano[2,3-C]pyrazole Derivatives. *Adv. Powder Technol.* 31, 1516–1528. doi:10.1016/j.apt.2020.01.012

Naji, S. Z., and Tye, C. T. (2022). A Review of the Synthesis of Activated Carbon for Biodiesel Production: Precursor, Preparation, and Modification. *Energy Convers. Manag. X* 13, 100152. doi:10.1016/j.ecmx.2021.100152

Pan, H., Li, H., Liu, X. F., Zhang, H., Yang, K. L., Huang, S., et al. (2016). Mesoporous Polymeric Solid Acid as Efficient Catalyst for (Trans)esterification of Crude Jatropha Curcas Oil. *Fuel Process. Technol.* 150, 50–57. doi:10.1016/j.fuproc.2016.04.035

Pan, H., Sun, J., Liu, J., Zhang, Y., and Zhou, S. (2021). Preparation of Sulfonated Carbon Derived from Orange Peel and its Application in Esterification. *Chem. Phys. Lett.* 770, 138395. doi:10.1016/j.cplett.2021.138395

Parreño, R. P., Liu, Y. L., Beltran, A. B., and Carandang, M. B. (2020). Effect of a Direct Sulfonation Reaction on the Functional Properties of Thermally-Crosslinked Electrospun Polybenzoxazine (PBz) Nanofibers. *RSC Adv.* 10, 14198–14207. doi:10.1039/d0ra01285h

Putra, M. D., Irawan, C., UdiantoroRistianingsih, Y., and Nata, I. F. (2018). A Cleaner Process for Biodiesel Production from Waste Cooking Oil Using Waste Materials as a Heterogeneous Catalyst and its Kinetic Study. *J. Clean. Prod.* 195, 1249–1258. doi:10.1016/j.jclepro.2018.06.010

Rokhum, S. L., Changmai, B., Kress, T., and Wheatley, A. E. H. (2022). A One-Pot Route to Tunable Sugar-Derived Sulfonated Carbon Catalysts for Sustainable Production of Biodiesel by Fatty Acid Esterification. *Renew. Energy* 184, 908–919. doi:10.1016/j.renene.2021.12.001

Safari, E., Rahemi, N., Kahforoushan, D., and Allahyari, S. (2019). Copper Adsorptive Removal from Aqueous Solution by Orange Peel Residue Carbon Nanoparticles Synthesized by Combustion Method Using Response Surface Methodology. *J. Environ. Chem. Eng.* 7, 102847. doi:10.1016/j.jece.2018.102847

Sangar, S. K., Syazwani, O. N., Farabi, M. S. A., Razali, S. M., Shobhana, G., Teo, S. H., et al. (2019). Effective Biodiesel Synthesis from Palm Fatty Acid Distillate (PFAD)using Carbon-Based Solid Acid Catalyst Derived Glycerol. *Renew. Energy* 142, 658–667. doi:10.1016/j.renene.2019.04.118

Sanjay, B. (2013). Heterogeneous Catalyst Derived from Natural Resources for Biodiesel Production : A Review. *Res. J. Chem. Sci.* 3, 95–101.

Seffati, K., Honarvar, B., Esmaeili, H., and Esfandiari, N. (2019). Enhanced Biodiesel Production from Chicken Fat Using CaO/CuFe2O4 Nanocatalyst and its Combination with Diesel to Improve Fuel Properties. *Fuel* 235, 1238–1244. doi:10.1016/j.fuel.2018.08.118

Sharma, S., Kundu, A., Basu, S., Shetti, N. P., and Aminabhavi, T. M. (2020). Sustainable Environmental Management and Related Biofuel Technologies. *J. Environ. Manage.* 273, 111096. doi:10.1016/j.jenvman.2020.111096

Tang, Z. E., Lim, S., Pang, Y. L., Ong, H. C., and Lee, K. T. (2018). Synthesis of Biomass as Heterogeneous Catalyst for Application in Biodiesel Production: State of the Art and Fundamental Review. *Renew. Sustain. Energy Rev.* 92, 235–253. doi:10.1016/j.rser.2018.04.056

Tariq, M., Ali, S., Ahmad, F., Ahmad, M., Zafar, M., Khalid, N., et al. (2011). Identification, FT-IR, NMR (1H and 13C) and GC/MS Studies of Fatty Acid Methyl Esters in Biodiesel from Rocket Seed Oil. *Fuel Process. Technol.* 92, 336–341. doi:10.1016/j.fuproc.2010.09.025

Thinnakorn, K., and Tscheikuna, J. (2014). Transesterification of Palm Olein Using Sodium Phosphate Impregnated on an Alumina Support. Appl. *Catal. A Gen.* 484, 122–133. doi:10.1016/j.apcata.2014.07.007

Thushari, I., Babel, S., and Samart, C. (2019). Biodiesel Production in an Autoclave Reactor Using Waste Palm Oil and Coconut Coir Husk Derived Catalyst. *Renew. Energy* 134, 125–134. doi:10.1016/j.renene.2018.11.030

Wan, H., Wu, Z., Chen, W., Guan, G., Cai, Y., Chen, C., et al. (2015). Heterogenization of Ionic Liquid Based on Mesoporous Material as Magnetically Recyclable Catalyst for Biodiesel Production. *J. Mol. Catal. A Chem.* 398, 127–132. doi:10.1016/j.molcata.2014.12.002

Wan, L., Chen, D., Liu, J., Zhang, Y., Chen, J., Du, C., et al. (2020). Facile Preparation of Porous Carbons Derived from Orange Peel via Basic Copper Carbonate Activation for Supercapacitors. *J. Alloys Compd.* 823, 153747. doi:10.1016/j.jallcom.2020.153747

Wang, A., Li, H., Pan, H., Zhang, H., Xu, F., Yu, Z., et al. (2018). Efficient and Green Production of Biodiesel Catalyzed by Recyclable Biomass-Derived Magnetic Acids. *Fuel Process. Technol.* 181, 259–267. doi:10.1016/j.fuproc.2018.10.003

Wang, M., Shi, R., Gao, M., Zhang, K., Deng, L., Fu, Q., et al. (2020). Sensitivity Fluorescent Switching Sensor for Cr (VI) and Ascorbic Acid Detection Based on Orange Peels-Derived Carbon Dots Modified with EDTA. *Food Chem.* 318, 126506. doi:10.1016/j.foodchem.2020.126506

Wang, Y. T., Fang, Z., and Zhang, F. (2019a). Esterification of Oleic Acid to Biodiesel Catalyzed by a Highly Acidic Carbonaceous Catalyst. *Catal. Today* 319, 172–181. doi:10.1016/j.cattod.2018.06.041

Wang, Y. T., Yang, X. X., Xu, J., Wang, H. L., Wang, Z. B., Zhang, L., et al. (2019b). Biodiesel Production from Esterification of Oleic Acid by a Sulfonated Magnetic Solid Acid Catalyst. *Renew. Energy* 139, 688–695. doi:10.1016/j.renene.2019.02.111

Yu, H., Cao, Y., Li, H., Zhao, G., Zhang, X., Cheng, S., et al. (2021). An Efficient Heterogeneous Acid Catalyst Derived from Waste Ginger Straw for Biodiesel Production. *Renew. Energy* 176, 533–542. doi:10.1016/j.renene.2021.05.098

Zhang, B., Gao, M., Geng, J., Cheng, Y., Wang, X., Wu, C., et al. (2021). Catalytic Performance and Deactivation Mechanism of a One-step Sulfonated Carbon-Based Solid-Acid Catalyst in an Esterification Reaction. *Renew. Energy* 164, 824–832. doi:10.1016/j.renene.2020.09.076

Zhang, H., Li, H., Hu, Y., Venkateswara Rao, K. T., (Charles) Xu, C., and Yang, S. (2019a). Advances in Production of Bio-Based Ester Fuels with Heterogeneous Bifunctional Catalysts. *Renew. Sustain. Energy Rev.* 114, 109296. doi:10.1016/j.rser.2019.109296

Zhang, H., Li, H., Xu, C. C., and Yang, S. (2019b). Heterogeneously Chemo/Enzyme-Functionalized Porous Polymeric Catalysts of High-Performance for Efficient Biodiesel Production. *ACS Catal.* 9, 10990–11029. doi:10.1021/acscatal.9b02748

Zhang, H., Zhou, Q., Chang, F., Pan, H., Liu, X. F., Li, H., et al. (2015). Production and Fuel Properties of Biodiesel from Firmiana Platanifolia L.F. As a Potential Non-food Oil Source. *Ind. Crops Prod.* 76, 768–771. doi:10.1016/j.indcrop.2015.08.002

Zhang, Y., Wong, W. T., and Yung, K. F. (2014). Biodiesel Production via Esterification of Oleic Acid Catalyzed by Chlorosulfonic Acid Modified Zirconia. *Appl. Energy* 116, 191–198. doi:10.1016/j.apenergy.2013.11.044

Zhou, Y., Niu, S., and Li, J. (2016). Activity of the Carbon-Based Heterogeneous Acid Catalyst Derived from Bamboo in Esterification of Oleic Acid with Ethanol. *Energy Convers. Manag.* 114, 188–196. doi:10.1016/j.enconman.2016.02.027

Zuo, D., Lane, J., Culy, D., Schultz, M., Pullar, A., and Waxman, M. (2013). Sulfonic Acid Functionalized Mesoporous SBA-15 Catalysts for Biodiesel Production. *Appl. Catal. B Environ.* 129, 342–350. doi:10.1016/J.APCATB.2012.09.029

Conflict of Interest: The authors declare that the research was conducted in the absence of any commercial or financial relationships that could be construed as a potential conflict of interest.

Publisher's Note: All claims expressed in this article are solely those of the authors and do not necessarily represent those of their affiliated organizations, or those of the publisher, the editors and the reviewers. Any product that may be evaluated in this article, or claim that may be made by its manufacturer, is not guaranteed or endorsed by the publisher.